galaxies

MDPI

Review

The IXPE Science of Pulsars and Their Nebulae

Niccolò Bucciantini [1,2,3,*], Roger W. Romani [4], Fei Xie [5,6] and Josephine Wong [4]

1 INAF Osservatorio Astrofisico di Arcetri, Largo Enrico Fermi 5, 50125 Firenze, Italy
2 Dipartimento di Fisica e Astronomia, Università degli Studi di Firenze, Via Sansone 1, 50019 Sesto Fiorentino, Italy
3 Istituto Nazionale di Fisica Nucleare, Sezione di Firenze, Via Sansone 1, 50019 Sesto Fiorentino, Italy
4 Department of Physics and Kavli Institute for Particle Astrophysics and Cosmology, Stanford University, Stanford, CA 94305, USA; rwr@astro.stanford.edu (R.W.R.); joswong@stanford.edu (J.W.)
5 Guangxi Key Laboratory for Relativistic Astrophysics, School of Physical Science and Technology, Guangxi University, Nanning 530004, China; xief@gxu.edu.cn
6 INAF Istituto di Astrofisica e Planetologia Spaziali, Via del Fosso del Cavaliere 100, 00133 Roma, Italy
* Correspondence: niccolo.bucciantini@inaf.it

Abstract: Pulsars (PSRs) and Pulsar Wind Nebulae (PWNe) form some of the most interesting high-energy astrophysical systems. Their prominent synchrotron emission makes them ideal candidates for polarimetry. Here, after briefly summarizing the scientific rationale underpinning the importance of their polarimetric studies, we review the current status and achievements obtained by the IXPE mission. For the first time, we have space- and phase-resolved X-ray data that allow us to set constraints on the geometry and level of turbulence of the magnetic field which, in turn, can help us to better understand which acceleration and radiation model(s) might be at work in these systems. Interestingly, PWNe show a large variety in terms of polarization degree that might indicate key physical differences, still to be further investigated.

Keywords: polarization; radiation mechanism: non-thermal; pulsars: general; supernova remnants; magnetic fields; X-rays: general

Citation: Bucciantini, N.; Romani, R.W.; Xie, F.; Wong, J. The IXPE Science of Pulsars and Their Nebulae. *Galaxies* **2024**, *12*, 45. https://doi.org/10.3390/galaxies12040045

Academic Editor:Margo Aller

Received: 28 June 2024
Revised: 26 July 2024
Accepted: 30 July 2024
Published: 7 August 2024

1. Introduction

Pulsars (PSRs) and Pulsar Wind Nebulae (PWNe) are among the foremost systems where high-energy astrophysical processes can be studied in great detail, and they have been at the forefront of recent theoretical and observational activity [1–3]. PSRs are the prototypical relativistic accelerators, and among the most efficient antimatter factories in the Universe [4,5]. Despite the recent improvements in the modeling of their magnetosphere [6–9], several questions remain unanswered, starting from the exact location of the radiating regions [10–13]. In this regard, the light-curve alone does not allow one to set robust constraints. On the contrary, polarization is far more constraining, with different models making strikingly different predictions on the phase-dependent pulse polarization properties [14,15]. Phase-resolved optical polarization measurements exist only for the Crab nebula [16] and PSR B0656 + 14 [17], and optical integrated polarimetry only for the Vela and B0540-69 PSRs [18,19]. In this respect, X-ray polarimetry can provide a substantial contribution: on the one hand, it allows us to check for possible energy dependence of the polarization properties that might indicate different radiation regions in the PSR magnetosphere; on the other hand, X-ray emissions, even if quite faint, are detected in the majority of young PSRs, as opposed to optical. For what concerns the physics of PWNe, the ability to probe the level of turbulence in the inner region might help us to understand which one of the many acceleration processes is operating. This is where high energy particles are expected to be accelerated, and where flaring and time variability are more prominent. In this respect, re-connection, diffusive shock acceleration, or the more recently suggested turbulent acceleration in the body of the nebula, make clearly distinctive predictions about the level of turbulence [20–22].

2. IXPE Science on PSR and PWNe

Despite major improvements in our understanding of PSR magnetospheres [5–9], the exact mechanism and location of the observed pulsed emission remain a mystery. There are some indications, based on pulse shape, that high-energy emission might originate close to the light cylinder or beyond. The diversity of the pulsar light-curves makes it hard to select a single model. One key aspect of existing models is that even if they can all be tuned to fit the light curve, their predictions in terms of polarization properties are substantially different. Models with emission regions located deep inside the light cylinder have, on average, a higher level of intrinsic polarization than models where emission is located at the light cylinder or in the striped wind [14,15,23,24]. Polarization is very sensitive to the magnetic geometry, while intensity seems to be a better tracer of the velocity at which plasma flows in the magnetosphere. Polarization measures are thus a far more constraining probe of the structure of the magnetosphere.

The most relevant current issue in the theory of young PWNe is the acceleration mechanism or mechanisms producing the observed broadband emission spectrum. The spectral energy distribution can be described from radio to MeV energies as a set of broken power-laws [1,25]. Particle-in-cell simulations of diffusive shock acceleration at the termination shock of relativistic and magnetized pair winds have shown that this is efficient only for very weak magnetization [20], in contrast to expectations from dynamical MHD modeling of the nebular structure. On the other hand, there is a current trend to invoke turbulence, either distributed in the nebula, or driven by re-connection at the shock itself, as a promising candidate [21,22]. Unfortunately, numerical simulations [26,27] have shown that synchrotron emission intensity maps are mostly sensitive to boosting but not to the level of turbulence in the plasma. Polarization offers us a unique opportunity to sample the level and location of turbulence within these systems. Comparison with polarimetric radio and optical data can also shed light on the possible origin of low energy particles.

3. Sources

During its first two years of operation, IXPE has observed five PWNe in the 2–8 keV energy range, chosen among the brightest and more extended. Here, we briefly summarize the current IXPE findings of four published targets.

3.1. Crab Nebula and Pulsar

The Crab PWN and its pulsar have been among the primary targets of the IXPE mission, in part because the nebula was the only object for which previous high significance measurements of X-ray polarization were available [28]. This system was observed in the first IXPE cycle for 80 ks, and it has been re-observed twice since, for a total exposure of 300 ks. Results from the first observation were reported by [29] (see Figure 1).

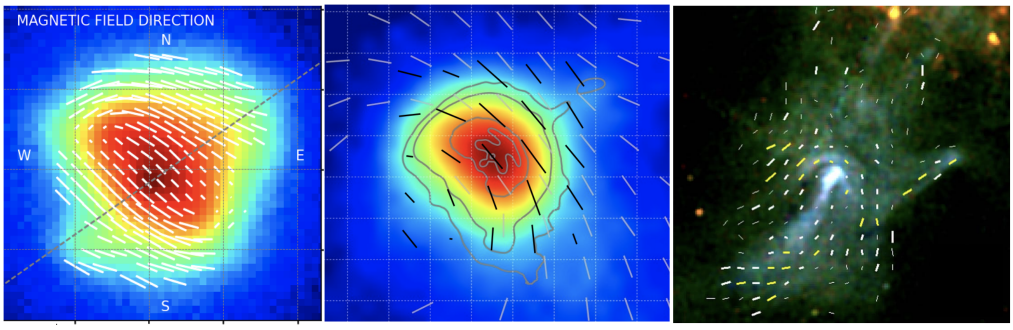

Figure 1. Magnetic field geometry, overlaid to the intensity, as measured by IXPE for the Crab nebula (**left**) from [29], Vela (**center**) from [30], and MSH 15−5^2 (**right**) from [31] (see the original papers for more details).

The integrated polarization degree (PD) was found to be 20%, in agreement with previous measurements, with a moderately significant change in the angle (PA = 145°, defined from the north to the east); not unexpected, given the large time span since previous observations and the variability of the PWN.

The polarization maps agree with the canonical expectation for synchrotron emission in a toroidal magnetic field (estimated nebular field strength in the range 100–150 μG) [32]. The symmetry axis agrees with the direction inferred from the shape of the emission torus. On the other hand, the map of polarization degree has a stronger level of asymmetry, with local regions in the North and South reaching PD $\sim$ 45%, indicating large variations in the amount of magnetic turbulence inside the PWN. No major trend with energy is found.

In a basic *on–off* analysis, the only phase bin where the PSR showed a polarization above the 3σ confidence level was at the center of the main peak, where the off-pulse subtracted emission gave normalized Stokes parameters, $Q/I = -0.132 \pm 0.025$ and $U/I = -0.079 \pm 0.025$, corresponding to PD of $15.4 \pm 2.5\%$ and PA $= 105^\circ \pm 18^\circ$. No significant change in the polarization properties with energy was found. The total phase-integrated PSR emission was found to be compatible with net zero polarization. Interestingly, the so-called *bridge* between the two peaks was found to have a low level of polarization, unlikely higher than $\sim$40% [14].

Wong et al., 2023 [33] re-analyzed the observation using a more sensitive technique called *simultaneous fitting*, in which one constructs models for the pulsar and nebula fluxes from high-resolution Chandra X-ray Observatory (*CXO*) observations, and uses them to solve for the pulsar phase-varying and nebula spatially varying polarization. Wong et al., 2024 [34] applied this method to the initial and follow-up observations. In the main peak, the PSR shows a PA monotonically increasing by $+40^\circ$, and a hump in PD that reaches a maximum of 15% at the bin before the peak phase. In both peaks, deviations greater than 1σ from optical polarization measurements taken by [16] were seen. A 3σ upper-limit PD $= 22\%$ was placed for the bridge polarization, confirming the low level of polarization seen in the first observation.

In the nebula polarization maps, high PD $\sim$ 45–50% in the North and South and a toroidal magnetic structure were again observed. Measurements in the jet suggest that the direction of the magnetic field relative to the jet flow changes from nearly perpendicular in the body to almost parallel at the tip, after the flow direction abruptly deflects by 90°. A spatial correlation between polarization degree and photon index was found. In particular, the western quadrant has the lowest polarization fraction and softest spectrum, while the southern quadrant has the opposite relation.

3.2. Vela

The Vela PWN is powered by a nearby young pulsar PSR B0833-45 (290 pc, spin-down age τ = 11,000 yr), and it is located inside its supernova remnant. High-resolution *CXO* images revealed two prominent arcs that are bisected by a jet and counter jet. Its X-ray size extends to around 1.6′ (the magnetic field is estimated to be $\sim$10 μG). IXPE observed the Vela PWN in April 2022 twice, with a total exposure of 860 ks. The detailed results are reported in [30,35] (see Figure 1).

The image-averaged PD in the 2–8 keV band was found to be notably high, $\sim$45%, which is twice higher than that of the Crab nebula. The measured PA was -50°, and this angle aligns with the symmetry axis of the Vela nebula.

Spatially resolved polarimetric measurements revealed a curved and symmetric PA pattern, showing a toroidal magnetic structure. At some regions, the polarization degree is $>$60%. Considering the PA variation observed over the whole nebula, we expect slightly higher local PD than the region-average value in each 30″ square region, which is limited by the angular resolution of IXPE. The measured high PD is close to the maximum value allowed for synchrotron emission with the observed X-ray spectrum, implying that the magnetic field is highly uniform across the emission region. The electrons in the PWN are accelerated with little or no turbulence in a highly uniform magnetic field.

Except for the center 'arc-jet' structure, a deeper *CXO* observation shows a faint, diffuse emission structure that extends toward the southwestern region with a scale of several arc minutes. This diffuse emission is highly polarized with a local PD $= 76.2 \pm 7.2\%$. The high PD suggests that the turbulent magnetic energy is, at most, 33% of the ordered one. On the other hand, observations in the radio band, at 5 GHz, display an extended image with two distinctive and asymmetric lobes. These lobes are located in the northeast and southwest of the central pulsar, with a diameter exceeding 10′ [36]. The radio nebula does not show significant features resembling the X-ray arc-jet structure observed in the central region. Instead, it primarily overlaps with the dim diffuse X-ray emission observed in the southwest region. Dodson et al. [36] showed the polarization map of the radio nebula, and a high PD of 60% was found. The observation revealed a large-scale toroidal magnetic field, which is remarkably consistent with the one seen in X-ray polarization, both in the center and the outskirts. This consistency reveals that the observed X-ray and radio emissions are produced by electrons in the same magnetic field. Unlike the Crab PWN, where radio polarimetry shows no evidence of a toroidal field, and no correlation with X-ray polarimetry [37], the consistency between radio and X-rays observed in the Vela PWN may be attributed to the interaction between the reverse shock of the supernova blast wave and the PWN, which leads to a displacement between the synchrotron-cooled outer nebula and the fresh nebula close to the pulsar.

3.3. MSH 15−5²

PSR B1509−58 is a young (spin-down age $\tau = 1600$ yr), energetic (spin-down power $\dot{E} = 1.7 \times 10^{37}$ erg s^{-1}), high field ($B_s = 1.5 \times 10^{13}$ G) pulsar embedded in the supernova remnant RCW89/MSH 15−5² (distance ∼5.5 kpc). This PWN, spanning ∼8′, has been spectacularly imaged by *CXO*, and is often called 'the cosmic hand'. IXPE observations in three epochs from September 2022 to March 2023 collected 1.5Ms of exposure, mapping the nebular polarization. The detailed results are reported in [31] (see Figure 1), but we summarize here the principal results for comparison with the other PWNe.

As for the Crab, *CXO* images of MSH 15−5²'s synchrotron X-rays show a sub-luminous elliptical zone, centered on the pulsar point source, surrounded to the northwest by bright arcs, which are interpreted as the termination shock in an equatorial flow (the nebular magnetic field is estimated in the range 10–30 μG). However, unlike the Crab, we do not see a corresponding arc to the southwest, so it is unclear whether these structures are imposed by a toroidal field, as in the Crab, or represent a bow-shock-like structure associated with pulsar motion and/or reverse shock compression. The southern polar outflow is particularly prominent for MSH 15−5². We will refer to it here as the 'jet' and, indeed, it may be similar to the Crab's polar jets, but it may also represent a bow-shock-confined trail in the central PWN. To the north, synchrotron X-rays show finger-like extensions, merging into the thermal X-ray emission of the surrounding supernova remnant.

While IXPE does not resolve the central sub-luminous zone, it does map the polarization across the arcs, jet, and finger regions. As expected, the inferred magnetic field follows the arc and aligns with the linear fingers. Similar polarization patterns are seen in the radio. Like the Crab and Vela, the linear X-ray polarization is remarkably strong, reaching PD $\sim 70^\circ$ in several regions. Again, we infer that, in the radiation zone at least, the PWN magnetic field is highly uniform. However, unlike Crab and Vela, the field is not dominated by a global toroidal component. This can likely be attributed to the SNR/reverse shock interaction. Perhaps most interesting is the polarization associated with the 'jet'. This X-ray bright structure is radio faint, and so IXPE provides a unique opportunity to probe its magnetic field. In this structure, the polarization degree increases with distance from the pulsar and the inferred magnetic field has a substantial angle to the local jet axis. One interpretation is that complex fields at the jet base mark the sites of particle acceleration, but that the field maintains a substantial helical component contributing to jet confinement, and smooths out toward the jet end, with little turbulence-induced fluctuations. None of this polarization behavior could have been traced without IXPE's imaging capabilities.

However, with MSH 15−5^2's complex 3-D structure, arc second-scale measurements of the X-ray polarization will be needed to fully map the cosmic hand.

The pulsed X-ray emission is significantly different from that of the Crab, with a broad peak likely representing a poorly resolved double peak (two broad pulses partly overlapping) offset from the broad radio peak. The present IXPE pulsar polarization measurement is too limited to constrain models directly, but coupled with the radio PA data, rotating vector models [38] suggest that the radio emission is in the normal mode [39]. However, the constraints are not strong, and additional X-ray polarization measures would help greatly in comparing the radio and X-ray emission altitudes and checking that the X-rays follow the radio dipole-inferred sweep.

3.4. SNR 0540-69

PSR B0540-69 is a young Crab-like pulsar located inside the supernova remnant B0540-69.3 in the Large Magellanic Cloud, a satellite galaxy of the Milky Way at a distance of ∼50 kpc. It has a short rotation period of 50 ms, a dipole spin-down age of ∼1500 yr, and a spin-down power $\dot{E} \sim 10^{38}$ erg s^{-1}. PSR B0540-69 is embedded in a bright PWN visible at wavelengths from the radio to the X-rays (the nebular magnetic field is estimated in the range 250–500 μG). As the fourth PWN and the first extragalactic example, IXPE observed it in three different periods, from December 2022 to May 2023, for a total exposure of ∼850 ks. The detailed results are reported in [40].

Due to the far distance, PSR B0540–69's X-ray nebula has an angular diameter of only 2″-3″, which is unresolved by IXPE. No statistically significant polarization is detected for the image-averaged complex (PSR and PWN), giving a 99% confidence polarization upper limit of 5.3%. A basic on–off analysis allows us to separate the PWN and PSR component, and detects polarization for both of them in the 4–6 keV energy range. For the PWN emission, defined as the off-pulse phases, a PD of 24.5% with PA = 78.1° is detected at a 4.6σ significance level, consistent with the PA observed in the optical and radio band. The measured PD is slightly higher than that of the Crab nebula, which may be due to the PWN being seen nearly edge-on. An interesting point is that, the nebular PA is at large angle to the spin-axis position angle derived from fitting the PWN morphology. On the other hand, for the Crab and Vela, it aligns well with the PWN symmetry axis. A possibility that leads to such large deviation of ∼90° in B0540-69 could be that the brighter axis in the *CXO* image selected as the torus in [41] is, instead, the jet.

For what concerns the PSR, in a single on-pulse window, a hint of polarization is measured at 3.8σ with PD = 50.0% and PA of 6.2°. A 'simultaneous' PSR/PWN analysis, the same method applied for the Crab, finds two bins at the edges of the pulse exceeding 3σ PD significance, with PD of 68% and 62%, and an error of 20%; intervening bins at 2–3σ significance have lower PD, hinting at possible depolarization structure.

4. Conclusions and Future Prospects

Thanks to IXPE, for the first time, we are in a position to investigate the magnetic field properties in the acceleration region of young PWNe, and to set constraints on the geometry of the magnetospheric emission in PSRs. Our findings show a large diversity in the polarization properties of PWNe, likely associated with differences in the acceleration mechanisms, and/or the level of interaction with the confining environment. This, in part, contrasts with the uniformity in the emission structure that has been observed. In particular, the high level of polarization found in Vela and MSH 15−5^2 is at odds with recent suggestions that turbulence can play a major role in these systems, in light of the fact that Vela is also an older system, likely subject to stronger interaction with the surrounding supernova remnant. In Crab, for example, the regions with the higher PD are found not in the center close to the PSR, but at the edge of the torus, unlike in optical [19]. Meanwhile, the overall large scale geometry is fully consistent with a toroidal field, unlike what is seen in radio, and the average polarization is found to be in the range 20–40%, with a large degree of variations. There are indications of possible magnetic dissipation taking

place along the jet of MSH $15-5^2$, and correlation between polarization and spectral index in the Crab nebula points to something similar. Current 2D MHD models of PWNe are totally unable to explain the observed integrated PD without introducing some ad hoc large level of turbulence in the body of the nebula, while 3D MHD models tend to over-predict the level of turbulence and are unable to produce even local PD higher than 20% (Olmi private communication). Our findings hint clearly that current models fail to capture some key properties in the dynamics of these systems, likely more tied to the interaction with the surrounding material. The high angular resolution of IXPE has also enabled us to perform polarization studies on the PSR, minimizing the PWN contribution, a key element to achieve significant results. Our findings suggest that PSRs are less polarized than what is predicted by inner magnetospheric models [14]. In the case of the Crab PSR, we find that X-ray and optical polarization differ at more than 1σ. There is substantial evidence that X-ray emission originates at higher altitudes and more likely at or beyond the light cylinder. In particular, the low level of polarization in the bridge of the Crab PSR contrasts with all predictions from inner magnetospheric models [14], while it looks more compatible with models placing the emission close or beyond the light cylinder, e.g., [11,23,24].

All in all, the combination of a large collecting area, high angular resolution, and an operating band coincident with that of *CXO* (enabling us to use its high resolution images as fiducial input, a key point for the approach used in, e.g., [33]) has enabled us to obtain space-and-phase resolved polarimetric information of both the nebula and PSR, going well beyond any previous attempt. It has, moreover, shown that PSRs are likely much less polarized that current inner magnetospheric models would have predicted, and more in line with models advocating emission from region closer to the light cylinder.

Author Contributions: This proceedings has been written on behalf of the IXPE collaboration, and of the Pulsar & Pulsar Wind Nebulae Topical Working Group, summarizing the current findings. All the authors have equally contributed. All authors have read and agreed to the published version of the manuscript.

Funding: This work was supported in part through NASA grant NNM17AA26C administered by the Marshall Space Flight Center. The Imaging X-ray Polarimetry Explorer (IXPE) is a joint US and Italian mission. The US contribution is supported by the National Aeronautics and Space Administration (NASA) and led and managed by its Marshall Space Flight Center (MSFC), with industry partner Ball Aerospace (contract NNM15AA18C). The Italian contribution is supported by the Italian Space Agency (Agenzia Spaziale Italiana, ASI) through contract ASI-OHBI-2022-13-I.0, agreements ASI-INAF-2022-19-HH.0 and ASI-INFN-2017.13-H0, and its Space Science Data Center (SSDC) with agreements ASI-INAF-2022-14-HH.0 and ASI-INFN 2021-43-HH.0, and by the Istituto Nazionale di Astrofisica (INAF) and the Istituto Nazionale di Fisica Nucleare (INFN) in Italy. N.B. was supported by the INAF MiniGrant "PWNnumpol—Numerical Studies of Pulsar Wind Nebulae in The Light of IXPE". F.X. is supported by National Natural Science Foundation of China (Grant No. 12373041).

Data Availability Statement: This research used data products provided by the IXPE Team (MSFC, SSDC, INAF, and INFN) and distributed with additional software tools by the High-Energy Astrophysics Science Archive Research Center (HEASARC), at NASA Goddard Space Flight Center (GSFC). Data for all observations are available in the HEASARC IXPE Data Archive (https://heasarc.gsfc.nasa.gov/docs/ixpe/archive/ (accessed on 1 August 2024)).

Conflicts of Interest: The authors declare no conflicts of interest.

Abbreviations

The following abbreviations are used in this manuscript:

CXO	Chandra X-ray Observatory
PWN	Pulsar Wind Nebula
PSR	Pulsar
PD	Polarization Degree
PA	Polarization Angle

References

1. Gaensler, B.M.; Slane, P.O. The Evolution and Structure of Pulsar Wind Nebulae. *Ann. Rev. Astron. Astrophys.* **2006**, *44*, 17–47. [CrossRef]
2. Kargaltsev, O.; Cerutti, B.; Lyubarsky, Y.; Striani, E. Pulsar-Wind Nebulae. Recent Progress in Observations and Theory. *Space Sci. Rev.* **2015**, *191*, 391–439. [CrossRef]
3. Amato, E. The Theory Of Pulsar Wind Nebulae: Recent Progress. In Proceedings of the High Energy Phenomena in Relativistic Outflows VII, Barcelona, Spain, 9–12 July 2019; p. 33. [CrossRef]
4. Blasi, P.; Amato, E. Positrons from pulsar winds. In *High-Energy Emission from Pulsars and their Systems, Proceedings of the First Session of the Sant Cugat Forum on Astrophysics, Catalonia, Spain, 12–16 April 2010*; Astrophysics and Space Science Proceedings; Springer: Berlin/Heidelberg, Germany, 2011; Volume 21, p. 624. [CrossRef]
5. Timokhin, A.N.; Harding, A.K. On the Maximum Pair Multiplicity of Pulsar Cascades. *Astrophys. J.* **2019**, *871*, 12. [CrossRef]
6. Li, J.; Spitkovsky, A.; Tchekhovskoy, A. Resistive Solutions for Pulsar Magnetospheres. *Astrophys. J.* **2012**, *746*, 60. [CrossRef]
7. Tchekhovskoy, A.; Spitkovsky, A.; Li, J.G. Time-dependent 3D magnetohydrodynamic pulsar magnetospheres: Oblique rotators. *Mon. Not. R. Astron. Soc. Lett.* **2013**, *435*, L1–L5. [CrossRef]
8. Philippov, A.A.; Spitkovsky, A.; Cerutti, B. Ab Initio Pulsar Magnetosphere: Three-dimensional Particle-in-cell Simulations of Oblique Pulsars. *Astrophys. J.* **2015**, *801*, L19. [CrossRef]
9. Cerutti, B.; Philippov, A.A.; Spitkovsky, A. Modelling high-energy pulsar light curves from first principles. *Mon. Not. R. Astron. Soc. Lett.* **2016**, *457*, 2401–2414. [CrossRef]
10. Pétri, J. High-energy emission from the pulsar striped wind: A synchrotron model for gamma-ray pulsars. *Mon. Not. R. Astron. Soc. Lett.* **2012**, *424*, 2023–2027. [CrossRef]
11. Pétri, J. Phase-resolved polarization properties of the pulsar striped wind synchrotron emission. *Mon. Not. R. Astron. Soc. Lett.* **2013**, *434*, 2636–2644. [CrossRef]
12. Kalapotharakos, C.; Brambilla, G.; Timokhin, A.; Harding, A.K.; Kazanas, D. Three-dimensional Kinetic Pulsar Magnetosphere Models: Connecting to Gamma-Ray Observations. *Astrophys. J.* **2018**, *857*, 44. [CrossRef]
13. Philippov, A.; Timokhin, A.; Spitkovsky, A. Origin of Pulsar Radio Emission. *Phys. Rev. Lett.* **2020**, *124*, 245101. [CrossRef] [PubMed]
14. Dyks, J.; Harding, A.K.; Rudak, B. Relativistic Effects and Polarization in Three High-Energy Pulsar Models. *Astrophys. J.* **2004**, *606*, 1125–1142. [CrossRef]
15. Pétri, J.; Kirk, J.G. The Polarization of High-Energy Pulsar Radiation in the Striped Wind Model. *Astrophys. J.* **2005**, *627*, L37–L40. [CrossRef]
16. Słowikowska, A.; Kanbach, G.; Kramer, M.; Stefanescu, A. Optical polarization of the Crab pulsar: Precision measurements and comparison to the radio emission. *Mon. Not. R. Astron. Soc. Lett.* **2009**, *397*, 103–123. [CrossRef]
17. Kern, B.; Martin, C.; Mazin, B.; Halpern, J.P. Optical Pulse-Phased Photopolarimetry of PSR B0656+14. *Astrophys. J.* **2003**, *597*, 1049–1058. [CrossRef]
18. Mignani, R.P.; Sartori, A.; de Luca, A.; Rudak, B.; Słowikowska, A.; Kanbach, G.; Caraveo, P.A. HST/WFPC2 observations of the LMC pulsar PSR B0540-69. *Astron. Astrophys.* **2010**, *515*, A110. [CrossRef]
19. Moran, P.; Mignani, R.P.; Shearer, A. HST optical polarimetry of the Vela pulsar and nebula. *Mon. Not. R. Astron. Soc. Lett.* **2014**, *445*, 835–844. [CrossRef]
20. Sironi, L.; Spitkovsky, A. Particle Acceleration in Relativistic Magnetized Collisionless Pair Shocks: Dependence of Shock Acceleration on Magnetic Obliquity. *Astrophys. J.* **2009**, *698*, 1523–1549. [CrossRef]
21. Sironi, L.; Spitkovsky, A. Acceleration of Particles at the Termination Shock of a Relativistic Striped Wind. *Astrophys. J.* **2011**, *741*, 39. [CrossRef]
22. Zrake, J.; Arons, J. Turbulent Magnetic Relaxation in Pulsar Wind Nebulae. *Astrophys. J.* **2017**, *847*, 57. [CrossRef]
23. Takata, J.; Chang, H.K. Pulse Profiles, Spectra, and Polarization Characteristics of Nonthermal Emissions from the Crab-like Pulsars. *Astrophys. J.* **2007**, *670*, 677–692. [CrossRef]
24. Harding, A.K.; Kalapotharakos, C. Multiwavelength Polarization of Rotation-powered Pulsars. *Astrophys. J.* **2017**, *840*, 73. [CrossRef]
25. Bühler, R.; Blandford, R. The surprising Crab pulsar and its nebula: A review. *Rep. Prog. Phys.* **2014**, *77*, 066901. [CrossRef]
26. Komissarov, S.S.; Lyubarsky, Y.E. The origin of peculiar jet-torus structure in the Crab nebula. *Mon. Not. R. Astron. Soc. Lett.* **2003**, *344*, L93–L96. [CrossRef]
27. Del Zanna, L.; Volpi, D.; Amato, E.; Bucciantini, N. Simulated synchrotron emission from pulsar wind nebulae. *Astron. Astrophys.* **2006**, *453*, 621–633. [CrossRef]
28. Weisskopf, M.C.; Silver, E.H.; Kestenbaum, H.L.; Long, K.S.; Novick, R. A precision measurement of the X-ray polarization of the Crab Nebula without pulsar contamination. *Astrophys. J.* **1978**, *220*, L117–L121. [CrossRef]
29. Bucciantini, N.; Ferrazzoli, R.; Bachetti, M.; Rankin, J.; Di Lalla, N.; Sgrò, C.; Omodei, N.; Kitaguchi, T.; Mizuno, T.; Gunji, S.; et al. Simultaneous space and phase resolved X-ray polarimetry of the Crab pulsar and nebula. *Nat. Astron.* **2023**, *7*, 602–610. [CrossRef]
30. Xie, F.; Di Marco, A.; La Monaca, F.; Liu, K.; Muleri, F.; Bucciantini, N.; Romani, R.W.; Costa, E.; Rankin, J.; Soffitta, P.; et al. Vela pulsar wind nebula X-rays are polarized to near the synchrotron limit. *Nature* **2022**, *612*, 658–660. [CrossRef]

31. Romani, R.W.; Wong, J.; Di Lalla, N.; Omodei, N.; Xie, F.; Ng, C.Y.; Ferrazzoli, R.; Di Marco, A.; Bucciantini, N.; Pilia, M.; et al. The Polarized Cosmic Hand: IXPE Observations of PSR B1509-58/MSH 15−5^2. *Astrophys. J.* **2023**, *957*, 23. [CrossRef]
32. Mizuno, T.; Ohno, H.; Watanabe, E.; Bucciantini, N.; Gunji, S.; Shibata, S.; Slane, P.; Weisskopf, M.C. Magnetic-field structure of the Crab pulsar wind nebula revealed with IXPE. *Publ. Astron. Soc. Jpn.* **2023**, *75*, 1298–1310. [CrossRef]
33. Wong, J.; Romani, R.W.; Dinsmore, J.T. Improved Measurements of the IXPE Crab Polarization. *Astrophys. J.* **2023**, *953*, 28. [CrossRef]
34. Wong, J.; Mizuno, T.; Bucciantini, N.; Romani, R.W.; Yang, Y.J.; Liu, K.; Deng, W.; Goya, K.; Xie, F.; Pilia, M.; et al. Analysis of Crab X-ray Polarization using Deeper IXPE Observations. *arXiv* **2024**, arXiv:2407.12779. [CrossRef]
35. Liu, K.; Xie, F.; Liu, Y.h.; Ng, C.Y.; Bucciantini, N.; Romani, R.W.; Weisskopf, M.C.; Costa, E.; Di Marco, A.; La Monaca, F.; et al. A Spatially Resolved X-ray Polarization Map of the Vela Pulsar Wind Nebula. *Astrophys. J.* **2023**, *959*, L2. [CrossRef]
36. Dodson, R.; Lewis, D.; McConnell, D.; Deshpande, A.A. The radio nebula surrounding the Vela pulsar. *Mon. Not. R. Astron. Soc. Lett.* **2003**, *343*, 116–124. [CrossRef]
37. Aumont, J.; Conversi, L.; Thum, C.; Wiesemeyer, H.; Falgarone, E.; Macías-Pérez, J.F.; Piacentini, F.; Pointecouteau, E.; Ponthieu, N.; Puget, J.L.; et al. Measurement of the Crab nebula polarization at 90 GHz as a calibrator for CMB experiments. *Astron. Astrophys.* **2010**, *514*, A70. [CrossRef]
38. Radhakrishnan, V.; Cooke, D.J. Magnetic Poles and the Polarization Structure of Pulsar Radiation. *Astrophys. Lett.* **1969**, *3*, 225.
39. Bartel, N.; Morris, D.; Sieber, W.; Hankins, T.H. The mode-switching phenomenon in pulsars. *Astrophys. J.* **1982**, *258*, 776–789. [CrossRef]
40. Xie, F.; Wong, J.; La Monaca, F.; Romani, R.W.; Heyl, J.; Kaaret, P.; Di Marco, A.; Bucciantini, N.; Liu, K.; Ng, C.Y.; et al. First Detection of Polarization in X-Rays for PSR B0540-69 and Its Nebula. *Astrophys. J.* **2024**, *962*, 92. [CrossRef]
41. Ng, C.Y.; Romani, R.W. Fitting Pulsar Wind Tori. II. Error Analysis and Applications. *Astrophys. J.* **2008**, *673*, 411–417. [CrossRef]